Electronic Supplementary Information

Structural reconfiguration of Ru-bearing high-entropy sulfide into efficient alkaline oxygen evolution catalyst

Wenfeng Peng[a,b*], Zhengxing Lv[c], Wenbo Cheng[b], Jiong Li[c], Shijing Zhao[b], Bingmin Yan[b], Lu Shang[d], Junshuang Zhou[e*], Tierui Zhang[d], Huiyang Gou[b*]

[a]College of Energy Engineering, Huanghuai University，Zhumadian 463000, China. E-mail: pengwenfeng@huanghuai.edu.cn
[b]Center for High Pressure Science and Technology Advanced Research, Beijing 100193, China. E-mail: huiyanggou@hpstar.ac.cn
[c]Shanghai Synchrotron Radiation Facility, Shanghai 201204, China
[d]Key Laboratory of Photochemical Conversion and Optoelectronic Materials, Technical Institute of Physics and Chemistry, Chinese Academy of Sciences, Beijing 100190, China
[e]School of Environmenial and Chemical Engineering, State Key Laboratory of Metastable Materials Science and Technology,Yanshan University, Qinhuangdao 066004, China.E-mail: junshuangzhou@126.com

Experimental Section

1. Materials synthesis

(FeCoNiCuRu)S_2, FeS_2, CoS_2, NiS_2 and RuS_2 were synthesized via a high-pressure, high-temperature (HPHT) approach using a cubic multi-anvil apparatus (Guilin, China). The experimental setup consisted of a graphite heating element, a pyrophyllite pressure medium, and a hexagonal boron nitride (h-BN) capsule. Initially, stoichiometric quantities of Ru, Cu, Ni, Co, Fe and S powders for each target composition were thoroughly ground for at least half an hour under an inert atmosphere within a glove box. These uniform mixtures were then compacted at 20 MPa into cylindrical precursors (5 mm in diameter × 3 mm in height), which were loaded into h-BN containers. Subsequently, these samples were exposed to 5.0 GPa pressure at 1500 °C for 15 minutes. Subsequently, the resulting solids were transformed into ultrafine powders via high-energy milling. This process involved 10 hours of planetary ball milling at 350 rpm in an argon atmosphere, with a 20:1 ball-to-powder ratio.

2. Structure characterizations

X-ray diffraction analysis of the synthesized sulfide was conducted using a PANalytical X'Pert Pro diffractometer with Cu Kα radiation, set to a scan rate of 0.013° per minute. The XRD patterns of (FeCoNiCuRu)S_2 were refined using Rietveld analysis in FullProf software. The morphology, structural characteristics, and compositional properties of the synthesized samples were analyzed by field-emission scanning electron microscopy (FESEM, JSM-7900F) and transmission electron microscopy (TEM, JEOL2010, Japan) integrated with energy-dispersive X-ray spectroscopy. High-resolution TEM (HRTEM) observations and elemental mapping were conducted at a voltage of 200 kV. Chemical states of the elements were identified by X-ray photoelectron spectroscopy (AXIS Ultra DLD) with an Al Kα source. XAS measurements were taken at both the Shanghai Synchrotron Radiation Facility (Beamline 11B) and the Canadian Light Source (HXMA beamline). The storage rings were maintained at 250 mA using a Si (111) double crystal monochromator, and calibrations were performed at the K-edges of Ni (8333 eV), Co (7709 eV), and Fe (7112 eV) foils. Operando XAS measurements targeting the Cu, Ni, Co and Fe K-edges in (FeCoNiCuRu)S_2 were acquired in fluorescence test mode. And the XAS data were processed with the ATHENA software subsequently evaluated using Artemis.

3. Electrode preparations

To prepare working electrodes, the synthesized catalyst (4 mg) was combined with 1 mL of a water-alcohol mixture (1:3 ratio by volume) and 30 μL of Nafion. And the resulting suspension was then sonicated for more than 30 minutes. Then, 12 μL of the resulting mixture was deposited onto a clean carbon cloth substrate (1 × 1 cm2), giving a catalyst mass density of 3 mg per square centimeter, followed by air-drying for no less than 30 minutes. For nickel foam (NF)-based supports, 1 × 1 cm2 sections of NF underwent ultrasonic cleaning in ethanol for half an hour, followed by drying. Subsequently, the catalyst ink was drop-cast onto the cleaned NF, yielding an approximate loading of 3.0 mg. The freshly coated NF electrodes were then allowed to air-dry for over five hours.

4. Electrochemical measurements

All electrochemical tests were conducted using a CHI760E workstation with a standard three-electrode configuration in 1.0 M KOH. The studied sample served as the working electrode, an

Hg/HgO electrode was employed as the reference electrode, and a carbon rod was utilized as the counter electrode. All potentials were converted to the reversible hydrogen electrode (RHE) scale using the equation: ERHE = E(Hg/HgO) + 0.098 + (0.095 × pH). Linear sweep voltammetry (LSV) was performed at a scan rate of 5 mV s-1. Electrochemical impedance spectroscopy (EIS) was performed over a frequency range spanning from 10^5 to 0.01 Hz. Additionally, cyclic voltammetry (CV) tests were carried out within the voltage window free from Faradaic reactions. Turnover frequency (TOF) of each electrocatalyst was determined according to: TOF = (j * A) / (z * F * n), where j is the current density, A is the geometric area of the electrode, z (with a value of 4) corresponds to the number of electrons involved in generating one mole of oxygen. The Faraday constant (F) and the total number of moles of metal ions (n) in the working electrode were also incorporated into the calculation.

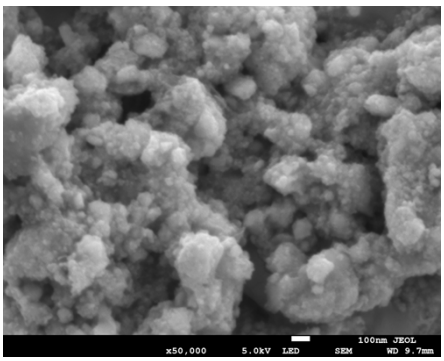

Figure S1: SEM result of (FeCoNiCuRu)S_2 after ball-milling.

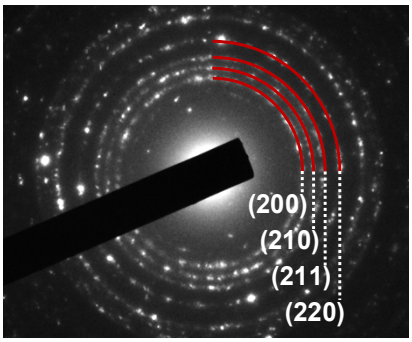

Figure S2: SAED pattern of (FeCoNiCuRu)S_2 after ball-milling.

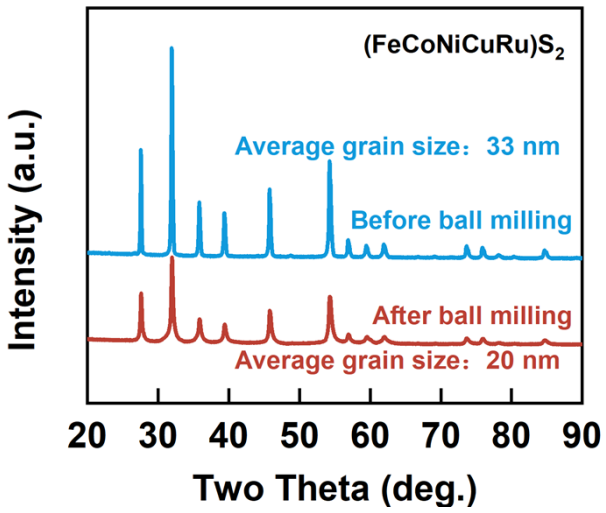

Figure S3: Comparison of the XRD patterns of $(FeCoNiCuRu)S_2$ before and after ball milling. The average grain size was obtained through analysis using the Scherrer formula:

$$D = (K\lambda)/(\beta \cos\theta)$$

where D represents the grain size, K is the Scherrer constant set at 0.89, λ is the X-ray wavelength taken as 0.15406 nm, β is the full width at half maximum (FWHM) of the diffraction peak, and θ is the diffraction angle. The grain sizes were calculated for the first six peaks, and the final average value was determined from these calculations.

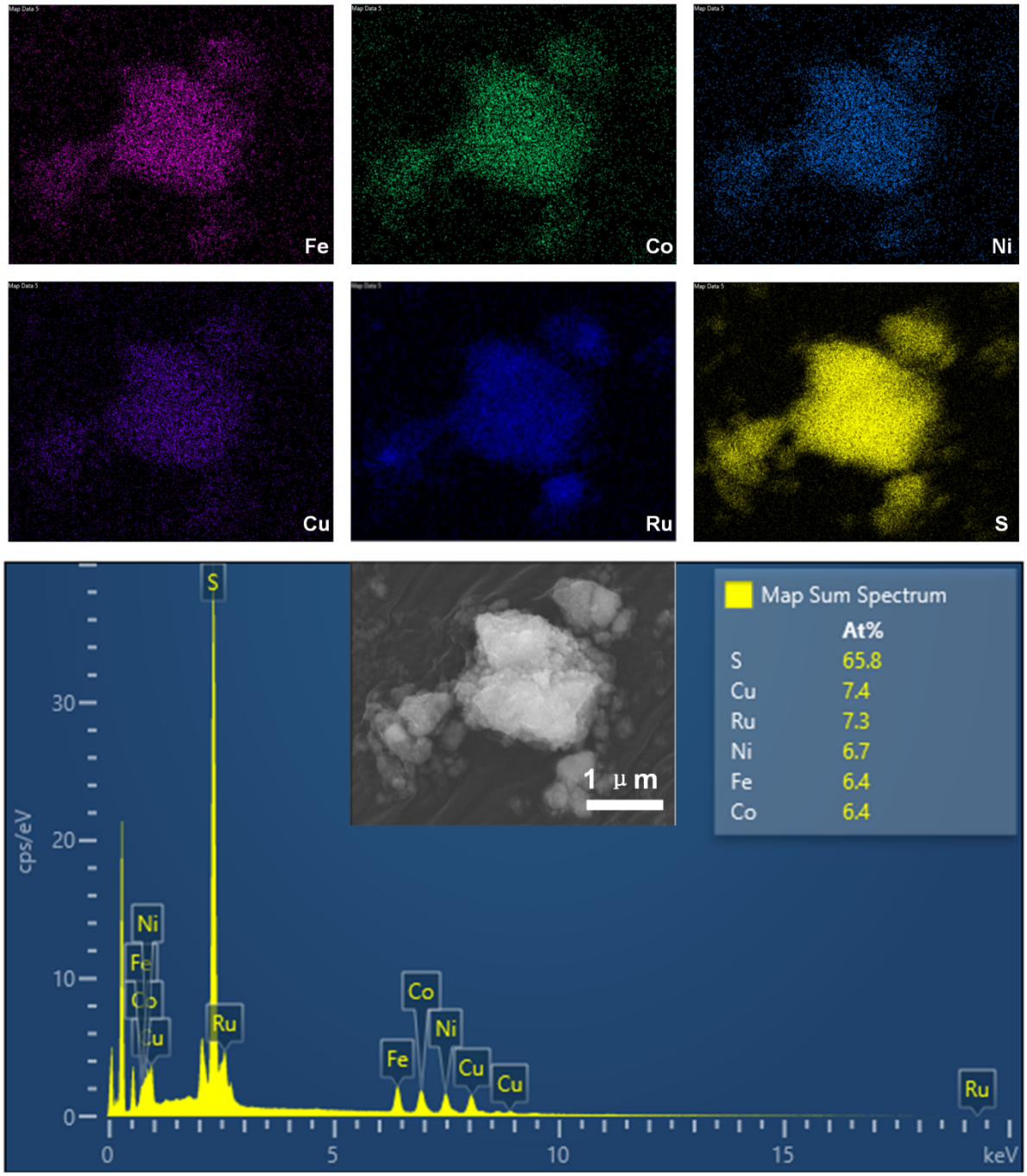

Figure S4: Energy dispersive X-ray elemental mapping and corresponding FESEM−EDX spectra for (FeCoNiCuRu)S_2 after ball-milling.

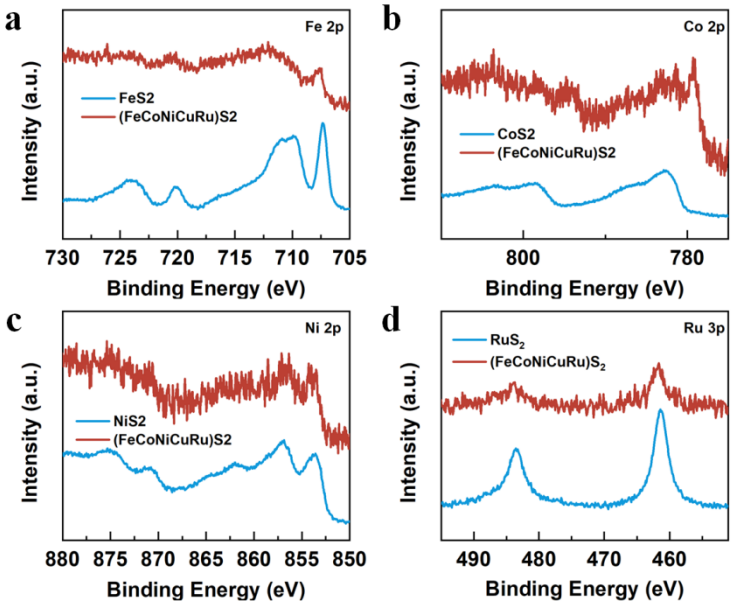

Figure S5: Comparison of the High-resolution XPS spectra of (FeCoNiCuRu)S_2 with that of FeS_2 (a), CoS_2 (b), NiS_2 (c) and RuS_2 (d).

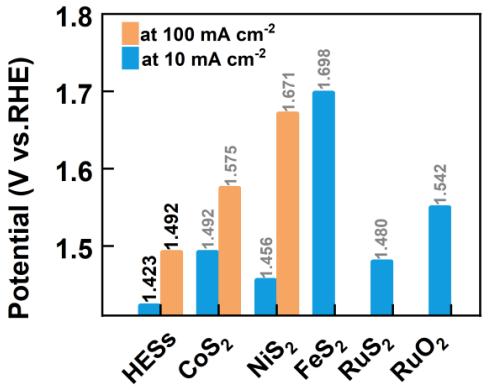

Figure S6: Comparison of the η_{10} and η_{100} among the synthesized metal sulfides and the reference RuO_2 electrocatalysts.

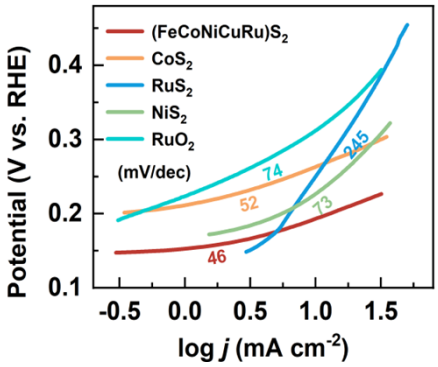

Figure S7: Tafel slopes of the synthesized metal sulfides and the reference RuO_2.

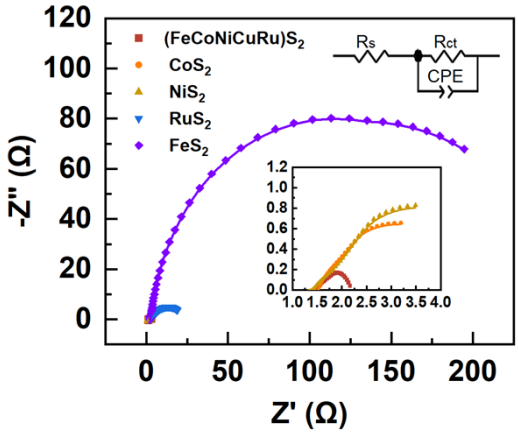

Figure S8: Electrochemical impedance spectroscopy of (FeCoNiCuRu)S_2, FeS_2, CoS_2, NiS_2 and RuS_2 deposited on carbon cloth with a mass density of 3.0 mg cm^{-2}. The partially enlarged view and the equivalent circuit is embedded in the Figure above.

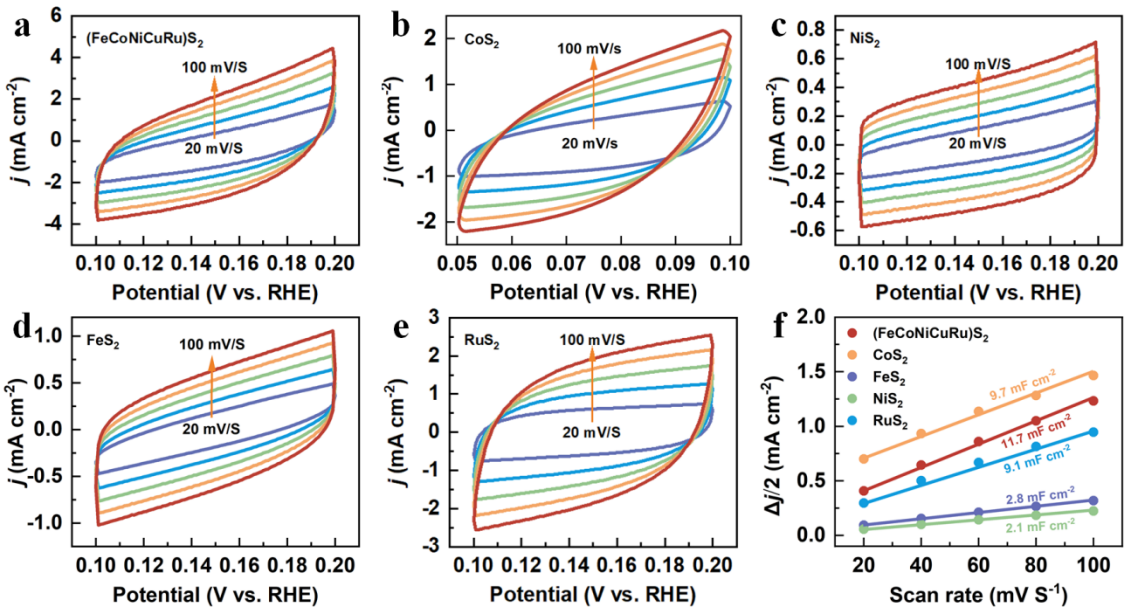

Figure S9: (a-e) Cyclic voltammetry (CV) curves and (f) derived electrochemical double-layer capacitance (C_{dl}) of (FeCoNiCuRu)S_2, CoS_2, NiS_2, FeS_2 and RuS_2.

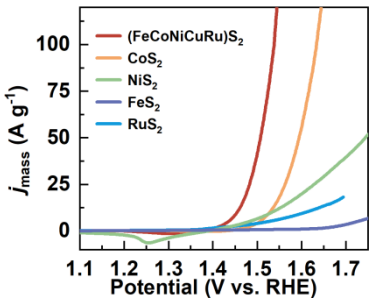

Figure S10: Mass activity of the synthesized sulfides sulfides.

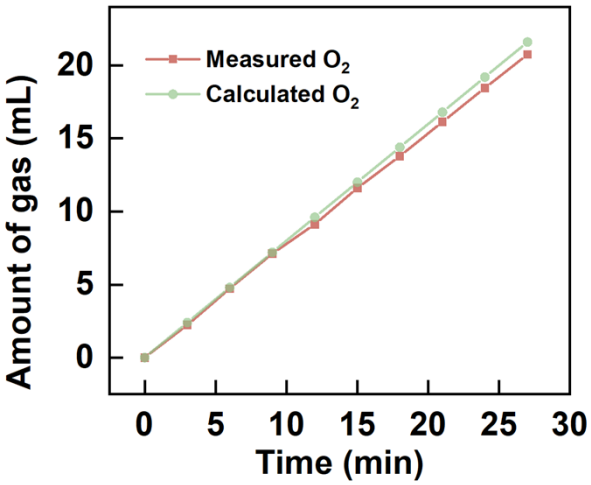

Figure S11: Comparison of the collected and theoretical gases for (FeCoNiCuRu)S_2.

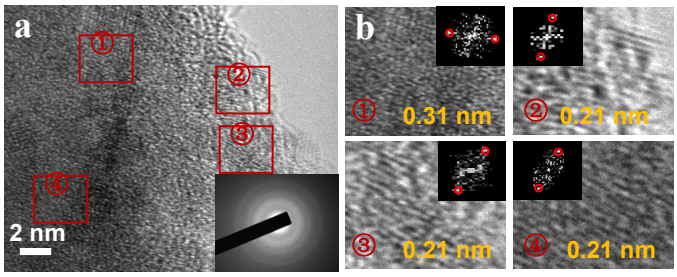

Figure S12: (a) HRTEM image and SAED pattern of (FeCoNiCuRu)S_2 after OER. (b) Local magnification of (a) marked with red rectangular wireframe.

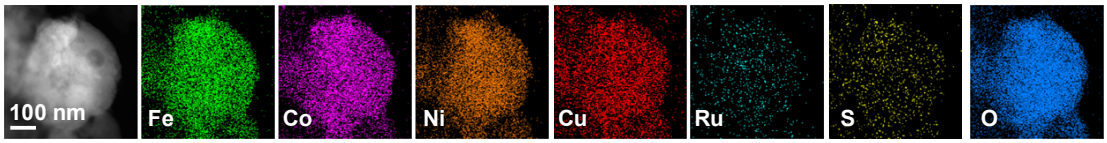

Figure S13: HAADF-STEM EDS mapping of (FeCoNiCuRu)S_2 after OER.

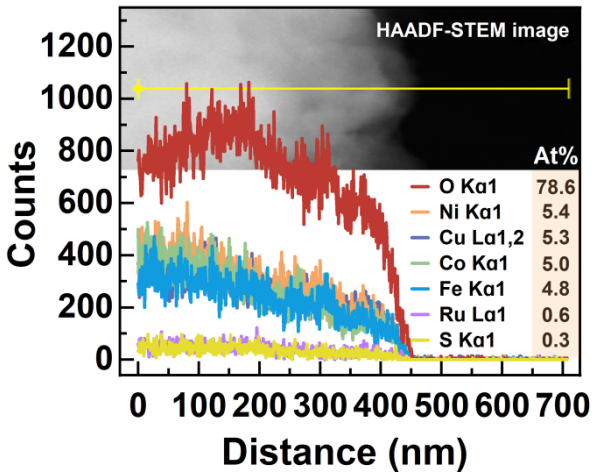

Figure S14: EDS line profiles of (FeCoNiCuRu)S_2 after OER test.

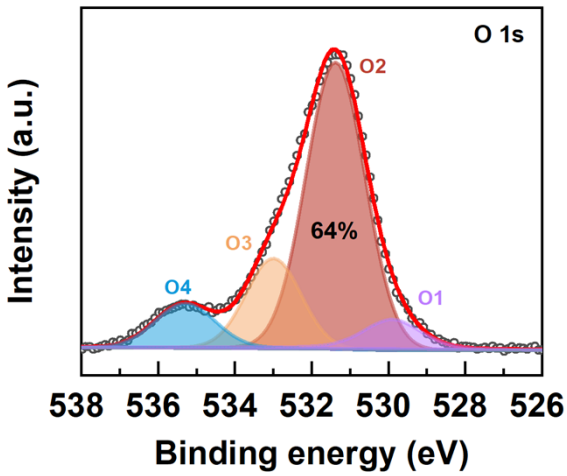

Figure S15: O 1s XPS spectra of (FeCoNiCuRu)S_2 after OER. O1 (529.5 eV), O2 (531.2 eV), O3 (533.1 eV), O4 (535.5 eV) are corresponding to the metal-oxygen bonds, defects, surface-adsorbed oxygen species, and chemisorbed oxygen respectively.

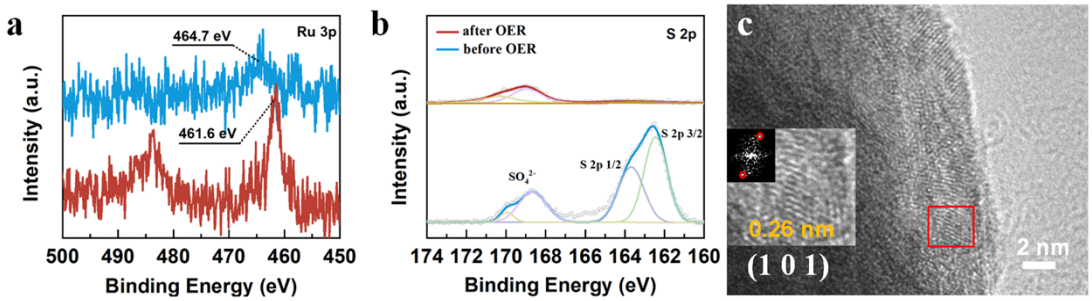

Figure S16: Ru 3p (a) and S 2p spectra (b) for (FeCoNiCuRu)S_2 before and after OER. (c) HRTEM image of (FeCoNiCuRu)S_2 after OER.

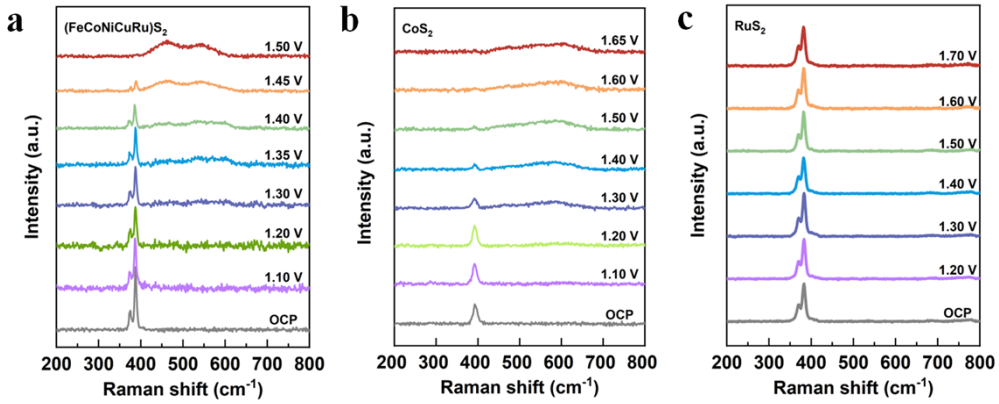

Figure S17: Operando Raman spectra of $(FeCoNiCuRu)S_2$ (a), CoS_2 (b), RuS2 (c) at various electrode potentials (V vs RHE) in alkaline electrolyte (1.0 M KOH).

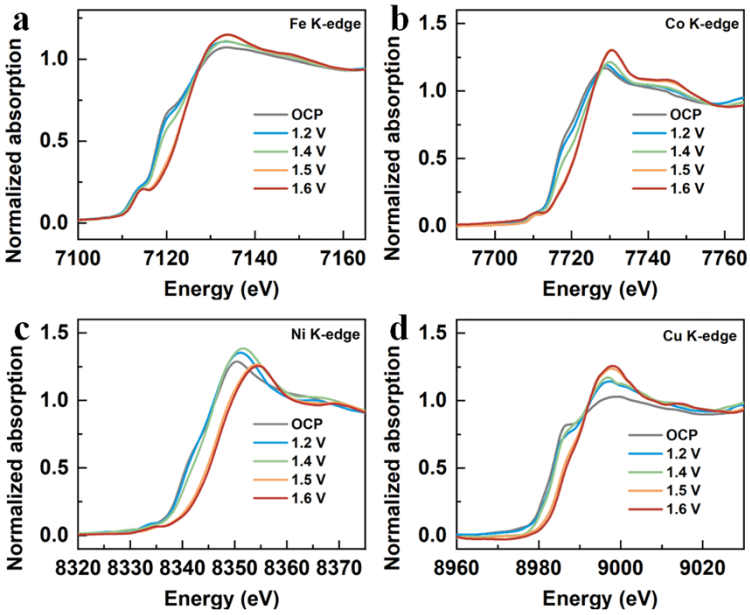

Figure S18: Operando Fe (a), Co (b), Ni (c) and Cu (d) K-edge XANES spectra of (FeCoNiCuRu)S_2 at varied potentials during the OER process, respectively.

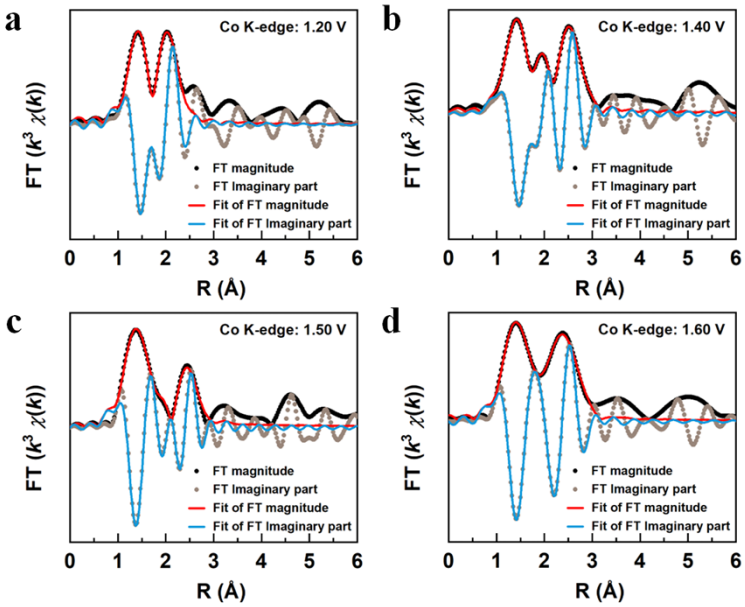

Figure S19. Fourier transformed k^3-weighted Co K edge EXAFS recorded for $(FeCoNiCuRu)S_2$ at 1.2 V RHE anodic (a), 1.4 V RHE anodic (b), 1.5 V RHE anodic (c) and 1.6 V RHE anodic (d). experimental data (circle) and the corresponding fitting (line).

Table S1. Chemical compositions detected by TEM-EDS of $(FeCoNiCuRu)S_2$ before OER test.

Sample	Elenmets	Weight (wt%)	Atom (at%)
$(FeCoNiCuRu)S_2$	Fe K	8.1	6.6
	Co K	8.8	6.8
	Ni K	9.1	7.1
	Cu K	10.6	7.6
	Ru K	18.6	8.4
	S K	44.8	63.5

Table S2. Comparison of OER performance of $(FeCoNiCuRu)S_2$ with similar reported systems in1.0 M KOH.

Catalyst	Mass density (mg/cm^2)	j ($mA\ cm^{-2}$)	η (mV)	Tafel slope ($mV\ dec^{-1}$)	Substrate	Ref.
$(FeCoNiCuRu)S_2$	**3.0**	**10** **100**	**193** **262**	**46**	**Carbon cloth**	**This work**
CoS_2 NS/CC	3.5	10	220	92	Carbon cloth	[1]
$FeCo_8S_8$ NS/rGO	5	10	290	72	Ni foam	[2]
$Fe_{11.8\%}$-Ni_3S_2/NF	7.9	100	253	65	Ni foam	[3]
MoO_x/Ni_3S_2	12	10	310	50	Ni foam	[4]
Ni_9S_8	11.04	10	340	109.8	Ni foam	[5]
Ni_3S_2/NF	/	10	340	150	Ni foam	[6]
$FeNiCoCrMnS_2$	2	10	199	39.1	Ni foam	[7]
$(Fe_{0.5}Ni_{0.5})S_2$	1.0	10	241	51.8	Carbon fiber cloth	[8]
Co-FeS_2/CoS_2	/	10	278	73	Carbon cloth	[9]
$Fe_{17.5\%}$-Ni_3S_2/NF	5	10	214	42	Ni foam	[10]
Cu-Ni_3S_2/Co_3S_4/NF	3.9	50	160	59.7	Ni foam	[11]
Co_9S_8@NOSC-900	5	20	330	/	Ni foam	[12]
CoS_2 HNSs	1.5	10	290	57	Carbon paper	[13]
$Ni_{0.85}Fe_{0.15}PS$	5	10	251	34	Ni foam	[14]
$FeWO_4$-Ni_3S_2@C/NF	/	10	200	39.4	Ni foam	[15]

Table S3. Fitting parameters of in-situ Fe, Co and Ni *K*-edge EXAFS spectra for $(FeCoNiCuRu)S_2$ catalyst at 1.60 V

	$(FeCoNiCuRu)S_2$ at 1.60 V				
	path	**CN**[a]	**R (Å)**[b]	**ΔE_o (eV)**[c]	**$\sigma^2(10^{-3}Å^2)$**[d]
Fe *K*-edge	Fe – O	3.0±0.2	1.95±0.02	-5.49	5.2
	Fe – M	1.0±0.4	2.89±0.04		5.0
Co *K*-edge	Co – O	4.8±0.2	1.88±0.04	-2.56	10.0
	Co – M	3.3±0.1	2.81±0.02		6.8
Ni *K*-edge	Ni – O	5.9±0.2	1.89±0.01	-5.16	6.9
	Ni – M	3.2±0.2	2.82±0.02		5.0

[a] the average coordination number CN. [b] R is the interatomic distance from the central scattering atom. [c] inner potential shift ΔE_o was set to equal and in a range of -6 to 6 eV. [d] Debye-Waller factor σ^2 was set in a range of 0.005 to 0.01. The Co (Fe, Ni) K edge EXAFS can be fitted with CoOOH structure.

Table S4. Chemical compositions detected by TEM-EDS of (FeCoNiCuRu)S2 after OER test.

Sample	Elenmets	Weight (wt%)	Atom (at%)
(FeCoNiCuRu)S_2	Fe K	10.5	4.9
	Co K	11.8	5.2
	Ni K	12.4	5.5
	Cu K	13.7	5.6
	Ru K	3.1	0.8
	S K	0.5	0.4
	O K	48.0	77.6

Table S5. Fitting parameters of in-situ Co K-edge EXAFS spectra for $(FeCoNiCuRu)S_2$ catalyst.

	$(FeCoNiCuRu)S_2$				
	path	**CN**	**R (Å)**	**ΔE_o (eV)**	**$\sigma^2(10^{-3}Å^2)$**
1.2 V	Co – O	2.6±0.1	1.89±0.01	-5.49	5.2
	Co – S	4.1±0.3	2.32±0.01		5.0
1.4 V	Co – O	3.8±0.2	1.89±0.02	1.80	4.8
	Co – S	1.2±0.1	2.31±0.02		4.6
	Co – $Co_{(CoOOH)}$	2.9±0.2	2.82±0.02		5.2
1.5 V	Co – O	4.0±0.3	1.89±0.02	-1.95	5.0
	Co – S	0.5±0.1	2.31±0.04		5.7
	Co – $Co_{(CoOOH)}$	3.1±0.1	2.82±0.01		8.2
1.6 V	Co – O	4.8±0.2	1.88±0.04	-2.56	10.0
	Co – $Co_{(CoOOH)}$	3.3±0.1	2.81±0.02		6.8

The EXAFS data at the Co K edge below 1.5 V are modeled using a $(FeCoNiCuRu)S_2$ + $Co(OH)_2$ model, while the data at 1.6 V apply exclusively to the CoOOH.

References for ESI

1. N. Yao, T. Tan, F. Yang, G. Cheng, W. Luo, Mater. Chem. Front. 2018, 2, 1732.

2. S. Lu, J. Jiang, H. Yang, Y. J. Zhang, D. N. Pei, J. J. Chen, Y. Yu, ACS nano 2020, 14, 10438.

3. N. Cheng, Q. Liu, A. M. Asiri, W. Xing, X. Sun, J. Mater. Chem. A 2015, 3, 23207-23212.

4. Y. Y. Wu, G. D. Li, Y. P. Liu, L. Yang, X. R. Lian, T. Asefa, X. X. Zou, Adv. Funct. Mater. 2016, 26, 4839-4847.

5. G. F. Chen, T. Y. Ma, Z. Q. Liu, N. Li, Y. Z. Su, K. Davey, S. Z. Qiao, Adv. Funct. Mater. 2016, 26, 3314-3323.

6. T. Zhu, L. Zhu, J. Wang, G. W. Ho, J. Mater. Chem. A 2016, 4, 13916.

7. T. X. Nguyen, Y. H. Su, C. C. Lin, J. M. Ting, Adv. Funct. Mater. 2021, 31, 2106229

8. W. Dai, Y. Pan, K. Ren, Y. A. Zhu, T. Lu, Electrochim. Acta 2020, 355, 136821.

9. K. Wang, W. Guo, S. Yan, H. Song, Y. Shi, RSC adv. 2018, 8, 28684.

10. G. Zhang, Y. S. Feng, W. T. Lu, D. He, C. Y. Wang, Y. K. Li, X. Y. Wang, F. F. Cao, ACS Catal. 2018, 8, 5431.

11. H. Su, S. Song, S. Li, Y. Gao, L. Ge, W. Song, T. Ma, J. Liu, Appl. Catal. B: Environ. 2021, 293, 120225.

12. S. Huang, Y. Meng, S. He, A. Goswami, Q. Wu, J. Li, S. Tong, T. Asefa, M. Wu, Adv. Funct. Mater. 2017, 27, 1606585.

13. X. Ma, W. Zhang, Y. Deng, C. Zhong, W. Hu, X. Han, Nanoscale 2018, 10, 4816.

14. W. Peng, J. Li, K. Shen, L. Zheng, H. Tang, Y. Gong, J. Zhou, N. Chen, S. Zhao, M. Chen, F. Gao, H. Gou, J. Mater. Chem. A 2020, 8, 23580-23589.

15. Z. Wang, G. Qian, T. Yu, J. Chen, F. Shen, L. Luo, Y. Zou, S. Yin, Chem. Eng. J. 2022, 134669.